## Infinite Grassmann Time-Evolving Matrix Product Operator Method in the Steady State

Chu Guo1,\* and Ruofan Chen2,†

<sup>1</sup>Key Laboratory of Low-Dimensional Quantum Structures and Quantum Control of Ministry of Education,
Department of Physics and Synergetic Innovation Center for Quantum Effects
and Applications, Hunan Normal University, Changsha 410081, China

<sup>2</sup>College of Physics and Electronic Engineering, and Center for Computational Sciences, Sichuan Normal University, Chengdu 610068, China
(Dated: April 2, 2024)

We present an infinite Grassmann time-evolving matrix product operator method for quantum impurity problems, which directly works in the steady state. The method embraces the well-established infinite matrix product state algorithms with the recently developed GTEMPO method, and benefits from both sides: it obtains numerically exact real-time Green's functions without sampling noises and bath discretization error, it is applicable for any temperature without the sign problem, its computational cost is independent of the transient dynamics and does not scale with the number of baths. We benchmark the method on the finite-temperature equilibrium Green's function in the noninteracting limit against exact solutions and in the single-orbital Anderson impurity model against GTEMPO calculations. We also study the zero-temperature non-equilibrium steady state of an impurity coupled to two baths with a voltage bias, obtaining consistent particle currents with existing calculations. The method is ideal for studying steady-state quantum transport, and can be readily used as an efficient real-time impurity solver in the dynamical mean field theory and its non-equilibrium extension.

Understanding non-equilibrium and open quantum phenomena is one of the major pursuits since the born of quantum physics. A prototypical microscopic model to describe these phenomena is the Anderson impurity model (AIM), where an impurity is coupled to one or several continuous, noninteracting baths of itinerant electrons [1]. By imposing a temperature or a voltage bias among the baths, the whole system of the impurity plus baths will be driven to a non-equilibrium steady state (NESS). The interplay between the strong local Coulomb interaction, the non-equilibrium driving and the dissipative effects of the bath could lead to very rich physical phenomena in the NESS [2–8].

A variety of numerical methods have been developed to study steady-state quantum transport [9–26], which could provide fairly accurate solutions in specific regimes. However, up to date there is no single method which could provide generally reliable and efficient solutions, as similar to the role played by the continuous-time Quantum Monte Carlo (CTQMC) methods in solving the equilibrium AIM in the imaginary-time axis [27–33].

The Grassmann time-evolving matrix product operator (GTEMPO) method, recently developed by us, is a promising candidate of this kind to solve the non-equilibrium quantum transport problem of the AIM [34]: it treats the bath exactly and obtains numerically exact results in the real-time axis without sampling noises; it is applicable for any temperature without the sign problem; most remarkably, its computational cost is independent of the number of baths, a feature that is ideal for studying quantum transport and is missing in most existing alternatives.

The power of GTEMPO can be understood through its formalism. Roughly speaking, its idea is somewhere in between the CTQMC methods and the conventional wave-function based methods where the impurity-bath state is parametrized by some wave function ansatz [35–53]. Similar to CTQMC, it integrates out the bath exactly. However, instead of sam-

pling from the perturbative expansion of the path integral (PI), GTEMPO directly represents the integrand of the PI as a Grassmann matrix product state (GMPS) non-perturbatively. Similar to the wave-function based methods, GTEMPO uses GMPS as its parametric ansatz, but only in the temporal domain for the multi-time impurity degrees of freedom. The computational cost of GTEMPO roughly scales as  $N^2 \chi^3$  for the single-orbital AIM, with N the discrete time steps and  $\chi$ the bond dimension of the GMPS. Importantly, for commonly used bath spectrum density, it is observed that  $\chi \approx 100$  could already give very accurate results [34, 54, 55], which underlies the efficiency of GTEMPO. However, to study steadystate quantum transport with GTEMPO, one needs to overcome the (usually very long) transient dynamics to reach the NESS first [56], as similar to the wave-function based methods [52, 53, 57], which sets a very large prefactor Nin the computational cost that could greatly hinder the efficiency. Here we also note the closely related tensor network IF method [65, 66], which represents the Feynman-Vernon IF per spin per bath as a fermionic MPS in the Fock state basis. therefore its computational cost scales exponentially with the number of baths.

In this work we propose an infinite GTEMPO (referred as iGTEMPO) method which directly targets at the steady state, eliminating the need for transient dynamics. The key insight is that in the infinite-time limit the memory of the initial state is lost, which is a situation that closely resembles an infinite many-body wave function where the boundary condition becomes irrelevant if one is only interested in the bulk. Therefore similar to the spatial case, one could use infinite GMPSs instead of finite ones to represent the multitime impurity steady states, in which only the tensors within a single time step need to be stored and manipulated. The iGTEMPO method seamlessly integrates the well-established infinite MPS techniques into the GTEMPO formalism. We benchmark its accuracy on the finite-temperature equilibrium

Green's function in the noninteracting limit against exact solutions, and in the single-orbital AIM against GTEMPO calculations. We also apply it to study the NESS of an impurity that is coupled to two zero-temperature baths with a voltage bias, where the obtained steady-state particle currents are consistent with existing calculations.

The GTEMPO Method. Before we introduce the iGTEMPO method, we first given an elementary review of the GTEMPO method in the real-time axis as they share most of the techniques in common. We will mainly focus on the single-orbital AIM (although both methods are directly applicable for general AIMs), where the impurity may be coupled to one bath (the equilibrium setup) or two baths (the non-equilibrium setup). The Hamiltonian is denoted as  $\hat{H} = \hat{H}_{imp} + \hat{H}_{int}$ , where  $\hat{H}_{imp} = (\epsilon_d - U/2) \sum_{\sigma} \hat{a}_{\sigma}^{\dagger} \hat{a}_{\sigma} + U \hat{a}_{\uparrow}^{\dagger} \hat{a}_{\uparrow} \hat{a}_{\downarrow}^{\dagger} \hat{a}_{\downarrow}$  is the impurity Hamiltonian with  $\epsilon_d$  the on-site energy and U the local Coulomb interaction,  $\hat{H}_{int} = \sum_{\nu,k,\sigma} \epsilon_k \hat{c}_{\nu,k,\sigma}^{\dagger} \hat{c}_{\nu,k,\sigma} + \sum_{\nu,k,\sigma} \left(V_{\nu,k} \hat{a}_{\sigma}^{\dagger} \hat{c}_{\nu,k,\sigma} + \text{H.c.}\right)$  contains the free bath Hamiltonians and the coupling between the impurity and the baths, characterized by the band energy  $\epsilon_k$  and the coupling strength  $V_{\nu,k}$  respectively. Here we have used  $\sigma \in \{\uparrow,\downarrow\}$  for spin indices, and  $\nu$  as the bath label.

The GTEMPO method is essentially a translation of the Grassmann PI into efficient GMPS operations. For real-time dynamics starting from a non-correlated impurity-bath initial state  $\hat{\rho}(0) = \hat{\rho}_{imp} \otimes \hat{\rho}_{bath}^{th}$ , where  $\hat{\rho}_{imp}$  is some impurity initial state and  $\hat{\rho}_{bath}^{th}$  is the bath equilibrium state, the corresponding path integral of the impurity partition function  $Z_{imp}(t) = \operatorname{Tr} \hat{\rho}(t)/\operatorname{Tr} \hat{\rho}_{bath}^{th}$  can be written as

$$Z_{\text{imp}}(t) = \int \mathcal{D}[\bar{\boldsymbol{a}}, \boldsymbol{a}] \mathcal{K}[\bar{\boldsymbol{a}}, \boldsymbol{a}] \prod_{\sigma} \mathcal{I}_{\sigma}[\bar{\boldsymbol{a}}_{\sigma}, \boldsymbol{a}_{\sigma}].$$
 (1)

Here  $\bar{a}_{\sigma}=\{\bar{a}_{\sigma}(\tau)\}$ ,  $a_{\sigma}=\{a_{\sigma}(\tau)\}$  are Grassmann trajectories [58] on the Keldysh contour [59–61], and  $\bar{a}=\{\bar{a}_{\uparrow},\bar{a}_{\downarrow}\}$ ,  $a=\{a_{\uparrow},a_{\downarrow}\}$ . The measure  $\mathcal{D}[\bar{a},a]=\prod_{\sigma,\tau}d\bar{a}_{\sigma}(\tau)da_{\sigma}(\tau)e^{-\bar{a}_{\sigma}(\tau)a_{\sigma}(\tau)}$ .  $\mathcal{I}_{\sigma}$  is the Feynman-Vernon influence functional (IF) [62] (noticing that  $\nu$  does not appear as a subscript of  $\mathcal{I}$ ), which, after discretization using the quasiadiabatic propagator path integral (QuaPI) method [63, 64] with a time step size  $\delta t$ , can be written as (up to time discretization error)

$$\mathcal{I}_{\sigma} \approx e^{-\sum_{\zeta,\zeta'} \sum_{j,k=1}^{N} \bar{a}_{\sigma,j}^{\zeta} \Delta_{j,k}^{\zeta\zeta'} a_{\sigma,k}^{\zeta'}}, \tag{2}$$

where  $N=t/\delta t$  is the total discrete time step,  $\zeta,\zeta'=\pm$  label the forward (+) and backward (-) Keldysh branches. The hybridization function  $\Delta_{j,k}^{\zeta\zeta'}=\sum_{\nu}\Delta_{\nu,j,k}^{\zeta\zeta'}$ , with  $\Delta_{\nu,j,k}^{\zeta\zeta'}$  being the hybridization function of bath  $\nu$  which is determined by the spectrum density  $J_{\nu}(\omega)=\sum_{k}V_{\nu,k}^{2}\delta(\omega-\omega_{k})$ .  $\mathcal{K}$  encodes the bare impurity dynamics that is only determined by  $\hat{\rho}_{\mathrm{imp}}$  and  $\hat{H}_{\mathrm{imp}}$ . After discretization,  $\mathcal{K}$  can be written as

$$\mathcal{K} = \langle -\boldsymbol{a} | \boldsymbol{a}_{N}^{+} \rangle \cdots \langle \boldsymbol{a}_{2}^{+} | \hat{U}_{\text{imp}} | \boldsymbol{a}_{1}^{+} \rangle \langle \boldsymbol{a}_{1}^{+} | \hat{\rho}_{\text{imp}} | \boldsymbol{a}_{1}^{-} \rangle \times \langle \boldsymbol{a}_{1}^{-} | \hat{U}_{\text{imp}}^{\dagger} | \boldsymbol{a}_{2}^{-} \rangle \times \cdots \times \langle \boldsymbol{a}_{N}^{-} | \boldsymbol{a} \rangle,$$
(3)

where  $a_k^{\pm}=\{a_{\uparrow,k}^{\pm},a_{\downarrow,k}^{\pm}\}$  and  $\hat{U}_{\mathrm{imp}}=e^{-\mathrm{i}\hat{H}_{\mathrm{imp}}\delta t},$   $\langle a_1^+|\hat{\rho}_{\mathrm{imp}}|a_1^-\rangle$  imposes the initial condition and the first and last terms on the rhs impose the boundary condition, e.g., the final trace operation in the impurity partition function.

The discretized  $\mathcal K$  and  $\mathcal I_\sigma$  are Grassmann tensors. They can be multiplied together using Grassmann tensor multiplications [34] to obtain  $\mathcal{A}[\bar{a}, a] = \mathcal{K}[\bar{a}, a] \prod_{\sigma} \mathcal{I}_{\sigma}[\bar{a}_{\sigma}, a_{\sigma}]$  as a single Grassmann tensor, which is the multi-time impurity state that encodes the whole information of the impurity dynamics, and is referred to as the augmented density tensor (ADT). In GTEMPO, one represents each K and  $I_{\sigma}$  as a GMPS, and then multiplies them together to obtain A as a GMPS (this multiplication is only performed on the fly using a zip-up algorithm for efficiency [34]). Based on A one can calculate any multi-time impurity correlations following the standard path integral formalism. For example, the greater Green's function between two time steps  $j, k \ (j > k)$  can be evaluated as  $iG_{\sigma}^{>}(j,k) = Z_{\mathrm{imp}}^{-1}(t) \int \mathcal{D}[\bar{\boldsymbol{a}},\boldsymbol{a}] a_{\sigma,j} \bar{a}_{\sigma,k} \mathcal{A}[\bar{\boldsymbol{a}},\boldsymbol{a}].$ In the zipup algorithm, this boils down to contracting a quasi-2D tensor network of size  $3 \times 8N$  [54]. Assuming that the bond dimension of the GMPS representation of each  $\mathcal{I}_{\sigma}$  (the MPS-IF) is  $\chi$ , then the computational cost to build each MPS-IF is roughly  $O(N^2\chi^3)$  using the partial IF algorithm [34] (which is improved to  $O(N\chi^4)$  using a more efficient strategy to build the MPS-IF [55]), and the computational cost to calculate one Green's function is roughly  $O(N\chi^2)$ .

When focusing on the NESS, unfortunately, the prefactor N in the cost of GTEMPO (as well as most of its alternatives) is usually huge to overcome the transient dynamics, which significantly hinders the computational efficiency and necessitates more effective approaches.

The iGTEMPO Method. To motivate the iGTEMPO method, we first note that each hybridization function  $\Delta_{j,k}^{\zeta\zeta'}$  in Eq.(2) is a single-variate function of the time difference j-k only, e.g.,  $\Delta_{j,k}^{\zeta\zeta'}=\eta_{j-k}^{\zeta\zeta'}$ . Therefore, the exponent of  $\mathcal{I}_{\sigma}$ , denoted as  $\mathcal{F}_{\sigma}=-\sum_{\zeta,\zeta'}\sum_{j,k=1}^N \bar{a}_{\sigma,j}^\zeta\Delta_{j,k}^{\zeta\zeta'}a_{\sigma,k}^{\zeta'}$ , is invariant under any shift of its time step indices, which closely resembles an infinite-range many-body Hamiltonian. This time-translationally invariant (TTI) property of  $\mathcal{F}_{\sigma}$  and thus  $\mathcal{I}_{\sigma}$  has a profound impact: they can be represented as infinite GMPSs where only the site tensors within a single time step are independent. In Ref. [55] we have explored this property and come up with an extremely efficient algorithm to build the  $\mathcal{I}_{\sigma}$  as a GMPS, which requires essentially only a constant number of GMPS multiplications. This algorithm can be easily adapted here to build the infinite GMPS representation of  $\mathcal{I}_{\sigma}$ .

However, the time-translational invariance of  $\mathcal{K}$  in Eq.(3) is broken by the initial condition  $\langle a_1^+|\hat{\rho}_{\mathrm{imp}}|a_1^-\rangle$ , which is the reason why open boundary GMPSs were used in the non-equilibrium setup [55]. Crucially, in the steady state the memory of the initial state is completely lost, which means that this term can be neglected in this limit. The bulk terms of  $\mathcal{K}$ , namely  $\langle a_{j+1}^+|\hat{U}_{\mathrm{imp}}|a_j^+\rangle$   $\langle a_j^-|\hat{U}_{\mathrm{imp}}^\dagger|a_{j+1}^-\rangle$ , are TTI under the shift of the time step index j, whereas the boundary condition is taken at the  $j=\infty$  limit. This is exactly the same situa-

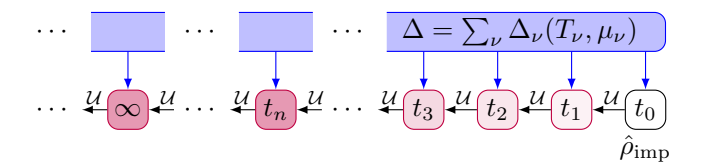


FIG. 1. Schematic demonstration of the infinite GTEMPO method that directly works in the steady state. The idea is that after a long quench from a non-correlated impurity-bath initial state, one loses the the memory of the transient dynamics. If one represents the discretized multi-time impurity dynamics as a Grassmann MPS, then for large t the tensors for each time step becomes exactly the same. Therefore if one is only interested in the steady state, one only needs to work with these time-translationally invariant tensors within a single time step, which could be obtained using well-established infinite MPS techniques. Here  $\mathcal U$  represents the discrete bare impurity dynamics propagator defined as  $\mathcal U[\hat \rho_{\rm imp}(t)] = \hat U_{\rm imp}\hat \rho_{\rm imp}(t)\hat U_{\rm imp}^{\dagger}$ .

tion as is met in case of a one-dimensional MPS with *infinite* boundary condition. Drawing this connection, we can represent  $\mathcal{K}$  as an infinite GMPS as well, and build it similar to the finite case but only perform the operations inside one unit cell. The idea of iGTEMPO is schematically shown in Fig. 1.

Implementation-wise, there are essentially only two functions that need to be reimplemented compared to GTEMPO. First, when constructing  $\mathcal K$  and  $\mathcal I_\sigma$  as infinite GMPSs, one needs to compress an infinite GMPS with a large dimension into a new one with a given bond dimension  $\chi$ . This can be done either deterministically using a series of singular value decompositions (SVDs) (SVD compression) [67], or iteratively such as using the infinite density matrix renormalization group (IDMRG) algorithm [68] or the variational uniform matrix product state (VUMPS) algorithm [69]. We have implemented the first two approaches, and tested them in our numerical examples. Second, after one has obtained the infinite GMPS representation of A (again A is only calculated on the fly), one needs to compute multi-time impurity correlations based on it. In GTEMPO, this is done by performing a left-to-right sweep, starting from and ending with trivial boundaries (the Grassmann vacuum 1), during which the conjugate pairs of GVs are integrated out [34, 54]. For infinite A, one needs to replace the boundaries by the left and right dominate eigenvectors of the transfer matrix, obtained by integrating out all the conjugate pairs of GVs within a unit cell. More implementation details about these two functions can be found in the Supplementary [70].

In the next we benchmark the iGTEMPO method with concrete numerical examples, mostly in terms of accuracy, as its performance advantage compared to GTEMPO (GTEMPO is already very efficient for transport problems [34]) is essentially the difference between finite and infinite MPS algorithms. For all our numerical simulations we will use a semicircular bath spectrum density  $J(\omega) = \Gamma D \sqrt{1-(\omega/D)^2}/2\pi$  with D=2 and  $\Gamma=0.1$  (we use  $\Gamma$  as the unit). We have also used IDMRG for infinite GMPS compression in the following numerical results as it is more efficient than SVD compres-

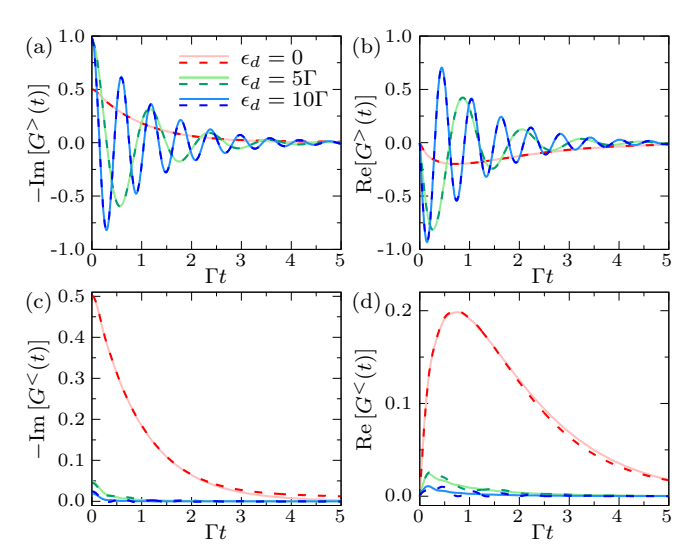


FIG. 2. (a) The real part and (b) the imaginary part of the equilibrium greater Green's function  $G^{>}(t)$  as a function of t. (c) The real part and (d) the imaginary part of the equilibrium lesser Green's function  $G^{<}(t)$  as a function of t. The red, green and blue dashed lines are iGTEMPO results for  $\epsilon_d/\Gamma=0,5,10$  respectively, the solid lines with the same colors are the corresponding ED results. We have used  $\Gamma\delta t=0.005,\, \chi=60$  and  $\beta=40$  in these simulations.

sion, whereas the comparison between these two compression algorithms can be found in the Supplementary [70].

Equilibrium Green's functions. We first validate iGTEMPO in the noninteracting limit against exact solutions. In Fig. 2, we compare the equilibrium greater and lesser Green's functions calculated using iGTEMPO (with  $\chi=60$  and  $\Gamma\delta t=0.005$ ) with exact diagonalization (ED) results calculated with  $\delta\omega/\Gamma=0.05$  (the bath discretization is the only error in ED, and we have verified that our ED results have well converged against  $\delta\omega$ ). We can see that the iGTEMPO results well agree with ED for different values of  $\epsilon_d$ , where the largest error is within 1% (See Supplementary for the convergence of iGTEMPO results against the bond dimension [70]).

Then we calculate the finite-temperature equilibrium retarded Green's function  $G(t) = G^{>}(t) - G^{<}(t)$  of the singleorbital AIM for which there does not exist exact solutions. Nevertheless, the GTEMPO results by calculating  $G(t-t_0)$ with  $\Gamma t_0 = 8$  (to overcome the transient dynamics) are already very accurate, since the impurity and bath have well reached equilibrium after  $t_0$  for the considered set of parameters [56]. In Fig. 3(a) we compared the iGTEMPO results with the GTEMPO results, for different values of  $U/\Gamma$  ranging from 1 to 9. We can see very good matches between these two sets of results for all Us. In Fig. 3(b) we show the spectral function  $A(\omega) = -\text{Im}[G(\omega)]/\pi$  where  $G(\omega)$  is the Fourier transformation of G(t). To calculated  $A(\omega)$  we have used linear prediction [71] to extend G(t) to very large t such that  $|G(t)| < 10^{-6}$ . To this end, we also note another advantage of (i)GTEMPO compared to both CTQMC and the wave-function based methods: once the  $\mathcal{I}_{\sigma}$ s have been built

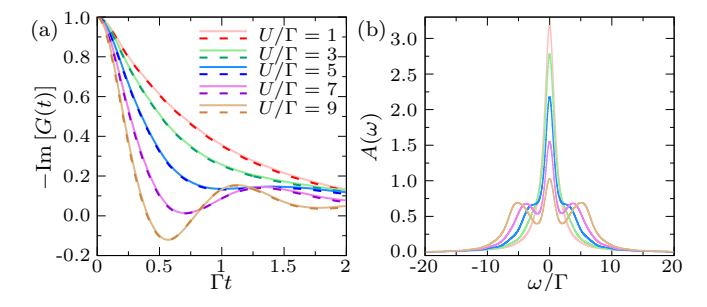


FIG. 3. (a) The imaginary part of the equilibrium retarded Green's function as a function of t for different values of U, where the solid and dashed lines are iGTEMPO and GTEMPO results respectively. For both iGTEMPO and GTEMPO we have used  $\Gamma \delta t = 0.005$ ,  $\chi = 60$  and  $\beta = 40$ . (b) The spectral function  $A(\omega)$  as a function of frequency  $\omega$ , obtained by taking the Fourier transformation of G(t).

as (infinite) GMPSs, they can be saved and used later with the Ks for different impurity Hamiltonians (the cost of building Ks is negligible) to compute the multi-time impurity correlations (as an example, the MPS-IFs for Fig. 3 are only calculated once for all different Us).

Non-equilibrium steady state. Finally, we calculate the NESS of an impurity coupled to baths with a voltage bias, an ideal application scenario for iGTEMPO. We consider the two baths at zero temperature with voltage bias  $\mu_1=-\mu_2=V/2$ , and compute the symmetrized steady-state particle current, defined as  $\mathcal{J}=(\mathcal{J}_{\uparrow}^1-\mathcal{J}_{\uparrow}^2)/2=(\mathcal{J}_{\downarrow}^1-\mathcal{J}_{\downarrow}^2)/2$ , where  $\mathcal{J}_{\sigma}^{\nu}$  denotes the particle current with spin  $\sigma$  that flows from the  $\nu$ th bath into the impurity. In the (i)GTEMPO methods, the particle current can be calculated as a summation of single particle Green's functions [34].

The steady-state particle current of this model has been calculated by an improved Quantum Monte Carlo (QMC) method [25], by the tensor network IF method till  $\Gamma t = 4.2$ (with  $\chi = 32$  and  $\Gamma \delta t = 0.007$ ) [66], by the GTEMPO method till  $\Gamma t = 4.2$  (with  $\chi = 160$ ,  $\Gamma \delta t = 0.007, 0.014$ ) [34] and till  $\Gamma t = 8.4$  (with  $\chi = 160$ ,  $\Gamma \delta t = 0.014$  for  $V/\Gamma < 1.1$ ) using a more efficient method to build the MPS-IF [55]. In the noninteracting limit with U=0, the GTEMPO results best agree with the ED results. In the interacting case, the time required to reach the steady state seems to be larger for smaller V and larger U, and it has been shown that the GTEMPO results have well converged for  $V/\Gamma \geq 1$  [55]. In Fig. 4, we show the steady-state particle current calculated by iGTEMPO, with comparisons to the existing calculations. We can see that the GTEMPO results calculated with  $\Gamma t = 8.4$  agree fairly well with the QMC results except for the points with  $V/\Gamma \approx 0.17$  and  $U/\Gamma > 2$  (the GTEMPO results for this point may have not converged yet with  $\Gamma t = 8.4$ ). The iGTEMPO results also agree fairly well with the QMC results, except for  $V/\Gamma \approx 0.17$  with  $U/\Gamma > 2$ and for  $V/\Gamma \approx 0.54, 0.71$  with  $U/\Gamma \geq 4$ , but it is not clear for now which set of results is more accurate at these points.

In summary, we have proposed an infinite Grassmann timeevolving matrix product operator (iGTEMPO) method which

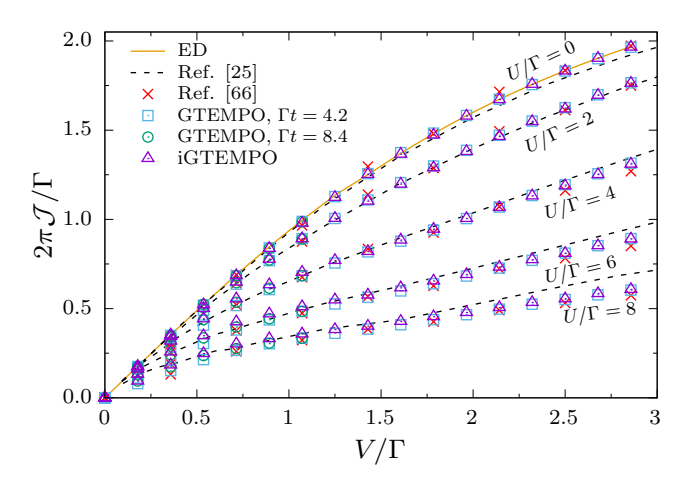


FIG. 4. The symmetrized steady-state particle current  $\mathcal J$  as a function of the voltage bias V for different values of U, calculated by ED (brown solid line for U=0), improved Quantum Monte Carlo [25] (black dashed line), tensor network IF till  $\Gamma t=4.2$  (with  $\chi=32$  and  $\Gamma \delta t=0.007$ ) [66] (red x), GTEMPO till  $\Gamma t=4.2$  (with  $\chi=160$  and  $\Gamma \delta t=0.007$ ) [34] (cyan square) and till  $\Gamma t=8.4$  (with  $\chi=160$  and  $\Gamma \delta t=0.014$ ) [55] (green circle), and iGTEMPO (purple triangle). For iGTEMPO we have used  $\chi=60$  and  $\Gamma \delta t=0.005$ .

makes use of the infinite Grassmann matrix product state to represent the multi-time impurity steady state. Similar to GTEMPO, iGTEMPO obtains numerically exact real-time Green's functions without sampling noises, applicable for any temperature without the sign problem, and its computational cost does not scale with the number of baths. Compared to GTEMPO or other non-sampling based methods, the infinite GMPS ansatz used in iGTEMPO is extremely compact: only the site tensors in a single time step is independent, and the total number of parameters only scale as  $16\chi^2$  for the singleorbital Anderson impurity model. The computational cost of iGTEMPO is essentially independent of the total evolution time, which roughly scales as  $O(\chi^3)$  for the single-orbital AIM. For the single-orbital AIM with the commonly used semi-circular spectrum in both the equilibrium (one bath) and non-equilibrium (two baths) setups, we show that with  $\chi = 60$ we can already obtain results with comparable precision to existing calculations. The iGTEMPO method is ideal for studying steady-state quantum transport problems, and can be readily used as a real-time impurity solver in the dynamical mean field theory (DMFT) [27] or non-equilibrium DMFT [6].

We thank Shiju Ran for helpful discussions on infinite MPS algorithms. This work is supported by National Natural Science Foundation of China under Grant No. 12104328. C. G. is supported by the Open Research Fund from State Key Laboratory of High Performance Computing of China (Grant No. 202201-00).

<sup>\*</sup> guochu604b@gmail.com

- † physcrf@sicnu.edu.cn
- [1] P. W. Anderson, Localized magnetic states in metals, Phys. Rev. **124**, 41 (1961).
- [2] M. H. Hettler, J. Kroha, and S. Hershfield, Nonequilibrium dynamics of the anderson impurity model, Phys. Rev. B 58, 5649 (1998).
- [3] L. Mühlbacher, D. F. Urban, and A. Komnik, Anderson impurity model in nonequilibrium: Analytical results versus quantum monte carlo data, Phys. Rev. B 83, 075107 (2011).
- [4] D. Becker, S. Weiss, M. Thorwart, and D. Pfannkuche, Non-equilibrium quantum dynamics of the magnetic anderson model, New J. Phys. 14, 073049 (2012).
- [5] G. Cohen, E. Gull, D. R. Reichman, A. J. Millis, and E. Rabani, Numerically exact long-time magnetization dynamics at the nonequilibrium kondo crossover of the anderson impurity model, Phys. Rev. B 87, 195108 (2013).
- [6] H. Aoki, N. Tsuji, M. Eckstein, M. Kollar, T. Oka, and P. Werner, Nonequilibrium dynamical mean-field theory and its applications, Rev. Mod. Phys. 86, 779 (2014).
- [7] A. Dorda, M. Ganahl, H. G. Evertz, W. von der Linden, and E. Arrigoni, Auxiliary master equation approach within matrix product states: Spectral properties of the nonequilibrium anderson impurity model, Phys. Rev. B 92, 125145 (2015).
- [8] D. M. Fugger, D. Bauernfeind, M. E. Sorantin, and E. Arrigoni, Nonequilibrium pseudogap anderson impurity model: a master equation tensor network approach, Phys. Rev. B 101, 165132 (2020).
- [9] A. Rosch, J. Paaske, J. Kroha, and P. Wölfle, Nonequilibrium transport through a kondo dot in a magnetic field: Perturbation theory and poor man's scaling, Phys. Rev. Lett. 90, 076804 (2003).
- [10] S. Kehrein, Scaling and decoherence in the nonequilibrium kondo model, Phys. Rev. Lett. 95, 056602 (2005).
- [11] S. G. Jakobs, V. Meden, and H. Schoeller, Nonequilibrium functional renormalization group for interacting quantum systems, Phys. Rev. Lett. 99, 150603 (2007).
- [12] E. Boulat, H. Saleur, and P. Schmitteckert, Twofold advance in the theoretical understanding of far-from-equilibrium properties of interacting nanostructures, Phys. Rev. Lett. 101, 140601 (2008).
- [13] F. B. Anders, Steady-state currents through nanodevices: A scattering-states numerical renormalization-group approach to open quantum systems, Phys. Rev. Lett. 101, 066804 (2008).
- [14] F. Heidrich-Meisner, A. E. Feiguin, and E. Dagotto, Real-time simulations of nonequilibrium transport in the single-impurity anderson model, Phys. Rev. B 79, 235336 (2009).
- [15] J. Eckel, F. Heidrich-Meisner, S. G. Jakobs, M. Thorwart, M. Pletyukhov, and R. Egger, Comparative study of theoretical methods for non-equilibrium quantum transport, New J. Phys. 12, 043042 (2010).
- [16] P. Werner, T. Oka, M. Eckstein, and A. J. Millis, Weak-coupling quantum monte carlo calculations on the keldysh contour: Theory and application to the current-voltage characteristics of the anderson model, Phys. Rev. B 81, 035108 (2010).
- [17] M. Pletyukhov and H. Schoeller, Nonequilibrium kondo model: Crossover from weak to strong coupling, Phys. Rev. Lett. 108, 260601 (2012).
- [18] S. Smirnov and M. Grifoni, Keldysh effective action theory for universal physics in spin-<sup>1</sup>/<sub>2</sub> kondo dots, Phys. Rev. B 87, 121302 (2013).
- [19] G. Cohen, E. Gull, D. R. Reichman, and A. J. Millis, Green's functions from real-time bold-line monte carlo calculations: Spectral properties of the nonequilibrium anderson impurity model, Phys. Rev. Lett. 112, 146802 (2014).

- [20] F. Reininghaus, M. Pletyukhov, and H. Schoeller, Kondo model in nonequilibrium: Interplay between voltage, temperature, and crossover from weak to strong coupling, Phys. Rev. B 90, 085121 (2014).
- [21] A. E. Antipov, Q. Dong, and E. Gull, Voltage quench dynamics of a kondo system, Phys. Rev. Lett. 116, 036801 (2016).
- [22] A. Erpenbeck, C. Hertlein, C. Schinabeck, and M. Thoss, Extending the hierarchical quantum master equation approach to low temperatures and realistic band structures, J. Chem. Phys. 149, 064106 (2018).
- [23] F. Schwarz, I. Weymann, J. von Delft, and A. Weichsel-baum, Nonequilibrium steady-state transport in quantum impurity models: A thermofield and quantum quench approach using matrix product states, Phys. Rev. Lett. 121, 137702 (2018).
- [24] M. Lotem, A. Weichselbaum, J. von Delft, and M. Goldstein, Renormalized lindblad driving: A numerically exact nonequilibrium quantum impurity solver, Phys. Rev. Res. 2, 043052 (2020).
- [25] C. Bertrand, S. Florens, O. Parcollet, and X. Waintal, Reconstructing nonequilibrium regimes of quantum many-body systems from the analytical structure of perturbative expansions, Phys. Rev. X 9, 041008 (2019).
- [26] A. Erpenbeck, E. Gull, and G. Cohen, Quantum monte carlo method in the steady state, Phys. Rev. Lett. 130, 186301 (2023).
- [27] E. Gull, A. J. Millis, A. I. Lichtenstein, A. N. Rubtsov, M. Troyer, and P. Werner, Continuous-time monte carlo methods for quantum impurity models, Rev. Mod. Phys. 83, 349 (2011).
- [28] A. N. Rubtsov, V. V. Savkin, and A. I. Lichtenstein, Continuoustime quantum monte carlo method for fermions, Phys. Rev. B 72, 035122 (2005).
- [29] E. Gull, P. Werner, O. Parcollet, and M. Troyer, Continuoustime auxiliary-field monte carlo for quantum impurity models, EPL 82, 57003 (2008).
- [30] P. Werner and A. J. Millis, Hybridization expansion impurity solver: General formulation and application to kondo lattice and two-orbital models, Phys. Rev. B 74, 155107 (2006).
- [31] P. Werner, A. Comanac, L. de' Medici, M. Troyer, and A. J. Millis, Continuous-time solver for quantum impurity models, Phys. Rev. Lett. 97, 076405 (2006).
- [32] H. Shinaoka, E. Gull, and P. Werner, Continuous-time hybridization expansion quantum impurity solver for multi-orbital systems with complex hybridizations, Comput. Phys. Commun. 215, 128 (2017).
- [33] E. Eidelstein, E. Gull, and G. Cohen, Multiorbital quantum impurity solver for general interactions and hybridizations, Phys. Rev. Lett. 124, 206405 (2020).
- [34] R. Chen, X. Xu, and C. Guo, Grassmann time-evolving matrix product operators for quantum impurity models, Phys. Rev. B 109, 045140 (2024).
- [35] M. Caffarel and W. Krauth, Exact diagonalization approach to correlated fermions in infinite dimensions: Mott transition and superconductivity, Phys. Rev. Lett. 72, 1545 (1994).
- [36] E. Koch, G. Sangiovanni, and O. Gunnarsson, Sum rules and bath parametrization for quantum cluster theories, Phys. Rev. B 78, 115102 (2008).
- [37] M. Granath and H. U. R. Strand, Distributional exact diagonalization formalism for quantum impurity models, Phys. Rev. B 86, 115111 (2012).
- [38] Y. Lu, M. Höppner, O. Gunnarsson, and M. W. Haverkort, Efficient real-frequency solver for dynamical mean-field theory, Phys. Rev. B 90, 085102 (2014).
- [39] C. Mejuto-Zaera, L. Zepeda-Núñez, M. Lindsey, N. Tubman,B. Whaley, and L. Lin, Efficient hybridization fitting for dy-

- namical mean-field theory via semi-definite relaxation, Phys. Rev. B **101**, 035143 (2020).
- [40] R.-Q. He and Z.-Y. Lu, Quantum renormalization groups based on natural orbitals, Phys. Rev. B 89, 085108 (2014).
- [41] R.-Q. He, J. Dai, and Z.-Y. Lu, Natural orbitals renormalization group approach to the two-impurity kondo critical point, Phys. Rev. B **91**, 155140 (2015).
- [42] F. A. Wolf, I. P. McCulloch, O. Parcollet, and U. Schollwöck, Chebyshev matrix product state impurity solver for dynamical mean-field theory, Phys. Rev. B 90, 115124 (2014).
- [43] M. Ganahl, P. Thunström, F. Verstraete, K. Held, and H. G. Evertz, Chebyshev expansion for impurity models using matrix product states, Phys. Rev. B 90, 045144 (2014).
- [44] M. Ganahl, M. Aichhorn, H. G. Evertz, P. Thunström, K. Held, and F. Verstraete, Efficient dmft impurity solver using real-time dynamics with matrix product states, Phys. Rev. B 92, 155132 (2015).
- [45] F. A. Wolf, A. Go, I. P. McCulloch, A. J. Millis, and U. Schollwöck, Imaginary-time matrix product state impurity solver for dynamical mean-field theory, Phys. Rev. X 5, 041032 (2015).
- [46] D. J. García, K. Hallberg, and M. J. Rozenberg, Dynamical mean field theory with the density matrix renormalization group, Phys. Rev. Lett. 93, 246403 (2004).
- [47] S. Nishimoto, F. Gebhard, and E. Jeckelmann, Dynamical mean-field theory calculation with the dynamical densitymatrix renormalization group, Physica B: Conden. Matter 378-380, 283 (2006), proceedings of the International Conference on Strongly Correlated Electron Systems.
- [48] A. Weichselbaum, F. Verstraete, U. Schollwöck, J. I. Cirac, and J. von Delft, Variational matrix-product-state approach to quantum impurity models, Phys. Rev. B 80, 165117 (2009).
- [49] D. Bauernfeind, M. Zingl, R. Triebl, M. Aichhorn, and H. G. Evertz, Fork tensor-product states: Efficient multiorbital realtime dmft solver, Phys. Rev. X 7, 031013 (2017).
- [50] Y. Lu, X. Cao, P. Hansmann, and M. W. Haverkort, Naturalorbital impurity solver and projection approach for green's functions, Phys. Rev. B 100, 115134 (2019).
- [51] D. Werner, J. Lotze, and E. Arrigoni, Configuration interaction based nonequilibrium steady state impurity solver, Phys. Rev. B 107, 075119 (2023).
- [52] L. Kohn and G. E. Santoro, Efficient mapping for anderson impurity problems with matrix product states, Phys. Rev. B 104, 014303 (2021).
- [53] L. Kohn and G. E. Santoro, Quench dynamics of the anderson impurity model at finite temperature using matrix product states: entanglement and bath dynamics, J. Stat. Mech. Theory Exp 2022, 063102 (2022).
- [54] R. Chen, X. Xu, and C. Guo, Grassmann time-evolving matrix product operators for equilibrium quantum impurity problems, New J. Phys. 26, 013019 (2024).

- [55] C. Guo and R. Chen, Efficient construction of the feynmanvernon influence functional as matrix product states, arXiv:2402.14350 (2024).
- [56] R. Chen, X. Xu, and C. Guo, Real-time impurity solver using grassmann time-evolving matrix product operators, arXiv:2401.04880 (2024).
- [57] B. Bauer, D. Wecker, A. J. Millis, M. B. Hastings, and M. Troyer, Hybrid quantum-classical approach to correlated materials, Phys. Rev. X 6, 031045 (2016).
- [58] J. W. Negele and H. Orland, Quantum Many-Particle Systems (Westview Press, 1998).
- [59] E. M. Lifshitz and L. P. Pitaevskii, Course of Theoretical Physics Volume 9: Statistical Physics part 2 (Elsevier, 1980).
- [60] J.-S. Wang, B. K. Agarwalla, H. Li, and J. Thingna, Nonequilibrium green's function method for quantum thermal transport, Front. Phys. 9, 673 (2013).
- [61] A. Kamenev and A. Levchenko, Keldysh technique and non-linear  $\sigma$ -model: Basic principles and applications, Adv. Phys. **58**, 197 (2009).
- [62] R. P. Feynman and F. L. Vernon, The theory of a general quantum system interacting with a linear dissipative system, Ann. Phys. 24, 118 (1963).
- [63] D. E. Makarov and N. Makri, Path integrals for dissipative systems by tensor multiplication. condensed phase quantum dynamics for arbitrarily long time, Chem. Phys. Lett. 221, 482 (1994).
- [64] N. Makri, Numerical path integral techniques for long time dynamics of quantum dissipative systems, J. Math. Phys. 36, 2430 (1995)
- [65] J. Thoenniss, A. Lerose, and D. A. Abanin, Nonequilibrium quantum impurity problems via matrix-product states in the temporal domain, Phys. Rev. B 107, 195101 (2023).
- [66] J. Thoenniss, M. Sonner, A. Lerose, and D. A. Abanin, Efficient method for quantum impurity problems out of equilibrium, Phys. Rev. B 107, L201115 (2023).
- [67] R. Orús and G. Vidal, Infinite time-evolving block decimation algorithm beyond unitary evolution, Phys. Rev. B 78, 155117 (2008).
- [68] I. P. McCulloch, Infinite size density matrix renormalization group, revisited, arXiv:0804.2509 (2008).
- [69] V. Zauner-Stauber, L. Vanderstraeten, M. T. Fishman, F. Verstraete, and J. Haegeman, Variational optimization algorithms for uniform matrix product states, Phys. Rev. B 97, 045145 (2018).
- [70] See supplementary material.
- [71] T. Barthel, U. Schollwöck, and S. R. White, Spectral functions in one-dimensional quantum systems at finite temperature using the density matrix renormalization group, Phys. Rev. B 79, 245101 (2009).

# **Supplementary Information: Infinite Grassmann Time-Evolving Matrix Product Operator Method** in the Steady State

Chu Guo<sup>1,\*</sup> and Ruofan Chen<sup>2,†</sup>

(Dated: April 2, 2024)

<sup>1</sup>Key Laboratory of Low-Dimensional Quantum Structures and Quantum Control of Ministry of Education,
Department of Physics and Synergetic Innovation Center for Quantum Effects
and Applications, Hunan Normal University, Changsha 410081, China
<sup>2</sup>College of Physics and Electronic Engineering, and Center for Computational Sciences, Sichuan Normal University, Chengdu 610068, China

# S.I. THE TIME-TRANSLATIONALLY INVARIANT APPROACH TO BUILD THE FEYNMAN-VERNON INFLUENCE FUNCTIONAL AS AN INFINITE GRASSMANN MATRIX PRODUCT STATE

As pointed out in the main text, the Feynman-Vernon influence functional (IF) is time-translationally invariant (TTI) and can be built as an infinite Grassmann matrix product state (GMPS). In the tensor network IF method [1], the Feynman-Vernon IF is built as a fermionic matrix product state (MPS) in the Fock state basis using the Fishman-White algorithm [2]. In the GTEMPO method, the Feynman-Vernon IF is built as a GMPS directly in the coherent state basis (which is the basis used for the analytical expression of the Feynman-Vernon IF) using the partial IF algorithm [3] by decomposing the IF into the product of a series of partial IFs, each with bond dimension 2 only. However, neither approach respects the TTI property of the IF. In Ref. [4], the TTI property of the Feynman-Vernon IF is explicitly explored, which results in a very efficient algorithm (referred to as the TTI-IF algorithm) that not only respects the time-translational invariance, but also requires only a constant number of GMPS multiplications. The TTI-IF algorithm proposed in Ref. [4] is used in the context of non-equilibrium real-time dynamics to build the finite GMPS representation of the IF (the usage of open boundary GMPS is because the bare impurity dynamics part  $\mathcal K$  is not TTI), nevertheless, the formalism of it can be readily used here to build the infinite GMPS representation of the IF. Here we will briefly review the major steps of the TTI-IF algorithm and point out the implementation-wise difference for the case of infinite GMPS.

We start from the discretized expression of the IF (Eq.(2) in the main text):

$$\mathcal{I}_{\sigma} \approx e^{-\sum_{\zeta,\zeta'} \sum_{j,k=1}^{N} \bar{a}_{\sigma,j}^{\zeta} \Delta_{j,k}^{\zeta\zeta'} a_{\sigma,k}^{\zeta'}},\tag{S1}$$

where N is the total number of discretely time steps,  $\Delta_{j,k}^{\zeta\zeta'}$  is the discretized hybridization matrix. In the finite case N is determined by the total evolution time, e.g.,  $N=t/\delta t$  for total time t and discrete time step size  $\delta t$ . In this work we directly focus on the steady state which is the infinite-time limit, and we will choose a larger enough N such that  $|\Delta_{j,j+N}^{\zeta\zeta'}| \approx 0$  (in our numerical implementation we require the absolute value to be less than  $10^{-6}$ ).

We denote the exponent in the discretized  $\mathcal{I}_{\sigma}$  as  $\mathcal{F}_{\sigma} = \sum_{\zeta,\zeta'} \mathcal{F}_{\sigma}^{\zeta\zeta'}$  with each  $\mathcal{F}_{\sigma}^{\zeta\zeta'}$ :

$$\mathcal{F}_{\sigma}^{\zeta\zeta'} = -\sum_{j,k=1}^{N} \bar{a}_{\sigma,j}^{\zeta} \Delta_{j,k}^{\zeta\zeta'} a_{\sigma,k}^{\zeta'}.$$
 (S2)

The TTI-IF algorithm contains two steps: (1) obtaining an efficient GMPS representation of  $e^{\delta \mathcal{F}}$  with  $\delta = 1/2^m$  a small positive number; (2) multiplying  $2^m$   $e^{\delta \mathcal{F}}$ s together to obtain  $\mathcal{I}_{\sigma}$ .

For the first step, we note that each hybridization matrix  $\Delta_{j,k}^{\zeta\zeta'}$  is actually a single-variate function of the time difference j-k, and  $\mathcal{F}_{\sigma}^{\zeta\zeta'}$  closely resembles a one-dimension translationally invariant many-body Hamiltonian. Therefore one could use the idea of constructing efficient infinite matrix product operator representation of translationally invariant Hamiltonians to built a compact GMPS representation of each  $\mathcal{F}_{\sigma}^{\zeta\zeta'}$ . Now we denote

$$\Delta_{j,k}^{\zeta\zeta'} = \eta_{j-k}^{\zeta\zeta'} \tag{S3}$$

<sup>\*</sup> guochu604b@gmail.com

<sup>†</sup> physcrf@sicnu.edu.cn

$$e^{\mathcal{F}/2^{m}} \cdots \xrightarrow{A_{\uparrow}^{a_{\uparrow}^{+}} A_{\bar{a}_{\uparrow}^{-}}^{\bar{a}_{\uparrow}^{+}} A_{\bar{a}_{\uparrow}^{-}}^{\bar{a}_{\uparrow}^{+}} A_{\bar{a}_{\downarrow}^{-}}^{\bar{a}_{\uparrow}^{+}} A_{\bar{a}_{\downarrow}^{-}}^{\bar{a}_{\downarrow}^{+}} \cdots$$

$$\downarrow copy$$

$$\cdots \xrightarrow{A_{\bar{a}_{\uparrow}^{+}}^{\bar{a}_{\uparrow}^{+}} A_{\bar{a}_{\uparrow}^{-}}^{\bar{a}_{\uparrow}^{+}} A_{\bar{a}_{\downarrow}^{-}}^{\bar{a}_{\uparrow}^{+}} A_{\bar{a}_{\downarrow}^{-}}^{\bar{a}_{\downarrow}^{-}} \cdots }$$

$$\downarrow copy$$

$$\cdots \xrightarrow{A_{\bar{a}_{\uparrow}^{+}}^{\bar{a}_{\uparrow}^{+}} A_{\bar{a}_{\uparrow}^{-}}^{\bar{a}_{\uparrow}^{+}} A_{\bar{a}_{\downarrow}^{-}}^{\bar{a}_{\uparrow}^{-}} A_{\bar{a}_{\downarrow}^{+}}^{\bar{a}_{\downarrow}^{+}} A_{\bar{a}_{\downarrow}^{-}}^{\bar{a}_{\downarrow}^{-}} \cdots }$$

FIG. S1. Schematic demonstration of the time-translationally invariant approach to build  $\mathcal{I}_{\sigma}$  as an infinite Grassmann MPS using m infinite GMPS multiplications (only the first step is shown here, since the rest m-1 steps are exactly the same as the first step), where MPS compression is performed after each multiplication.

to explicit stress the TTI property of the hybridization matrix. We can use the Prony algorithm [5] to find an optimal expansion of  $\eta_{i-k}^{\zeta\zeta'}$  as the summation of n exponential functions as

$$\eta_x^{\zeta\zeta'} \approx \sum_{l=1}^n \alpha_l \lambda_l^{|x|},$$
(S4)

for both x > 0 (for terms in Eq.(S2) with j > k) and x < 0 (for terms in Eq.(S2) with j < k). Once the optimal values of  $\alpha_l$  and  $\lambda_l$  are obtained, we can construct  $\mathcal{F}_{\sigma}^{\zeta\zeta'}$  as a TTI GMPS whose site tensors are:

$$\begin{bmatrix} 1 & \alpha_{1}a_{\sigma}^{\zeta'} & \cdots & \alpha_{n}a_{\sigma}^{\zeta'} & -\bar{\alpha}_{1}\bar{a}_{\sigma}^{\zeta} & \cdots & -\bar{\alpha}_{n}\bar{a}_{\sigma}^{\zeta} & \eta_{0}^{\zeta\zeta'}a_{\sigma}^{\zeta'}\bar{a}_{\sigma}^{\zeta} \\ 0 & \lambda_{1} & \cdots & 0 & 0 & \cdots & 0 & \lambda_{1}\bar{a}_{\sigma}^{\zeta} \\ \vdots & \vdots & \cdots & \vdots & \vdots & \cdots & \vdots & \vdots \\ 0 & 0 & \cdots & \lambda_{n} & 0 & \cdots & 0 & \lambda_{n}\bar{a}_{\sigma}^{\zeta} \\ 0 & 0 & \cdots & 0 & \bar{\lambda}_{1} & \cdots & 0 & \bar{\lambda}_{1}a_{\sigma}^{\zeta'} \\ \vdots & \vdots & \cdots & \vdots & \vdots & \cdots & \vdots & \vdots \\ 0 & 0 & \cdots & 0 & 0 & \cdots & \bar{\lambda}_{n} & \bar{\lambda}_{n}a_{\sigma}^{\zeta'} \\ 0 & 0 & \cdots & 0 & 0 & \cdots & 0 & 1 \end{bmatrix},$$
(S5)

where  $\alpha_l$  and  $\lambda_l$  correspond to the expansion of  $\eta_x^{\zeta\zeta'}$  for  $1 \le x \le N$  in Eq.(S4), while  $\bar{\alpha}_l$  and  $\bar{\lambda}_l$  correspond to the expansion of  $\eta_x^{\zeta\zeta'}$  for  $-N \le x \le -1$ . For infinite GTEMPO (iGTEMPO), the only formal difference with the finite case considered in Ref. [4] is that Eq.(S5) is understood as the site tensor of an infinite GMPS, while in Ref. [4] it is understood as the site tensor of an open boundary GMPS. Here we also notice that Eq.(S5) contains two Grassmann variables (GVs),  $\alpha_\sigma^{\zeta'}$  and  $\bar{\alpha}_\sigma^{\zeta}$ , therefore if one represents each GV with a site tensor (which is the case in our implementation), then Eq.(S5) represents a two-site tensor which needs to be split into two tensors in practice. With the infinite GMPS representation of each  $\mathcal{F}_\sigma^{\zeta\zeta'}$ , one can immediately obtain a first-order approximation of  $e^{\delta\mathcal{F}_\sigma^{\zeta\zeta'}}$ , using the W<sup>I</sup> algorithm [6] for example, which is an infinite GMPS with bond dimension 2n+1, with TTI site tensors:

$$\begin{bmatrix} 1 + \delta \eta_0^{\zeta\zeta'} a_\sigma^{\zeta'} \bar{a}_\sigma^{\zeta} & \sqrt{\delta} \alpha_1 a_\sigma^{\zeta'} & \cdots & \sqrt{\delta} \alpha_n a_\sigma^{\zeta'} & -\sqrt{\delta} \bar{\alpha}_1 \bar{a}_\sigma^{\zeta} & \cdots & -\sqrt{\delta} \bar{\alpha}_n \bar{a}_\sigma^{\zeta} \\ \sqrt{\delta} \lambda_1 \bar{a}_\sigma^{\zeta} & \lambda_1 & \cdots & 0 & 0 & \cdots & 0 \\ \vdots & \vdots & \cdots & \vdots & \vdots & \cdots & \vdots \\ \sqrt{\delta} \lambda_n \bar{a}_\sigma^{\zeta} & 0 & \cdots & \lambda_n & 0 & \cdots & 0 \\ \sqrt{\delta} \bar{\lambda}_1 a_\sigma^{\zeta'} & 0 & \cdots & 0 & \bar{\lambda}_1 & \cdots & 0 \\ \vdots & \cdots & \vdots & \vdots & \cdots & \vdots & \vdots \\ \sqrt{\delta} \bar{\lambda}_n a_\sigma^{\zeta'} & 0 & \cdots & 0 & 0 & \cdots & \bar{\lambda}_n \end{bmatrix}. \tag{S6}$$

In practice we use the slightly more sophisticated  $W^{II}$  method instead, which results in an infinite GMPS with the same bond dimension but is a more accurate first-order approximation [6].

Once we have obtained efficient infinite GMPS representations of the four  $e^{\delta \mathcal{F}_{\sigma}^{\zeta'}}$ 's (for the four choices of  $\zeta\zeta'$ ), we can multiply them together using infinite GMPS multiplications (which can be implemented in exactly the same as as finite GMPS multiplication [3]) to obtain  $e^{\delta\mathcal{F}_{\sigma}}$  as an infinite GMPS, during which infinite GMPS compression is done to compress the result infinite GMPS into a given bond dimension  $\chi$  (the algorithm of compressing an infinite GMPS will be described later). With  $e^{\delta\mathcal{F}_{\sigma}}$ , Ref. [4] introduces an extremely efficient algorithm to build  $\mathcal{I}_{\sigma}$  as a GMPS using only m GMPS multiplications, which

(a) 
$$\langle v_l | \underbrace{ \begin{pmatrix} \lambda a_r^+ + \bar{a}_r^- + \bar{a$$

FIG. S2. Algorithm to calculate the Green's functions based on the infinite Grassmann MPS representation of the augmented density tensor, which can be done in two steps: (a) Computing the transfer matrix by integrating out the conjugate pairs of Grassmann variables in a unit cell, and then calculating the left and right dominant eigenstates of it; (b) Identifying a finite window from the infinite ADT depending on the Green's function to be calculated, and then evaluating the Green's function similar to the finite case, but with nontrivial left and right boundary vectors obtained from step (a). The single-orbital Anderson impurity model with 8 Grassmann variables per unit cell is used for demonstration of the algorithm.

can be directly used here except that we deal with infinite GMPSs instead: in the *i*th step we multiply  $e^{\mathcal{F}_{\sigma}/2^{m-i+1}}$  with itself. This TTI-IF algorithm for building the infinite GMPS representation of  $\mathcal{I}_{\sigma}$  is schematically shown in Fig. S1.

There are two additional sources of error in the TTI-IF algorithm on top of the time discretization error and the MPS bond truncation error (the latter two are the only sources of errors in the partial IF algorithm), namely the error occurred in the Prony algorithm and the error in the first order approximation of  $e^{\delta \mathcal{F}_{\sigma}}$ . The Prony algorithm is a well studied algorithm in signal processing and can often converge with an n that only scales logarithmically with N [7–10]. The second source of error clearly decays exponentially with m for the design of the algorithm. In all the simulations of this work, we require the mean square error occurred in the Prony algorithm to be less than  $10^{-5}$  and set m=5 (the same as in Ref. [4]), which gives very accurate results for the model settings we have considered.

#### S.II. CALCULATING MULTI-TIME IMPURITY CORRELATIONS

Once we have obtained the infinite GMPS representations of  $\mathcal{K}$  and  $\mathcal{I}$ , we can further multiply them together to obtain the augmented density tensor (ADT):  $\mathcal{A}\left[\bar{a},a\right]=\mathcal{K}\left[\bar{a},a\right]\prod_{\sigma}\mathcal{I}_{\sigma}\left[\bar{a}_{\sigma},a_{\sigma}\right]$ , as an infinite GMPS (this multiplication is only performed on the fly using the zipup algorithm as in the finite case [3]). Then one can easily calculate any multi-time correlations of the impurity. For example, the greater and lesser Green's functions can be calculated as

$$iG_{j}^{>} = iG_{j,0}^{>} = \langle \hat{a}_{j}\hat{a}_{0}^{\dagger} \rangle = \langle e^{-i\hat{H}j\delta t}\hat{a}e^{i\hat{H}j\delta t}\hat{a}^{\dagger} \rangle = Z_{\rm imp}^{-1} \int \mathcal{D}[\bar{\boldsymbol{a}}, \boldsymbol{a}]a_{j}\bar{a}_{0}\mathcal{A}[\bar{\boldsymbol{a}}, \boldsymbol{a}]; \tag{S7}$$

$$-\mathrm{i}G_{j}^{<} = -\mathrm{i}G_{j,0}^{<} = \langle \hat{a}_{0}^{\dagger}\hat{a}_{j} \rangle = \langle \hat{a}^{\dagger}e^{-\mathrm{i}\hat{H}j\delta t}\hat{a}e^{\mathrm{i}\hat{H}j\delta t} \rangle = Z_{\mathrm{imp}}^{-1} \int \mathcal{D}[\bar{\boldsymbol{a}}, \boldsymbol{a}]\bar{a}_{0}a_{j}\mathcal{A}[\bar{\boldsymbol{a}}, \boldsymbol{a}], \tag{S8}$$

where the TTI property of the steady-state greater and lesser Green's functions has been used in the first equalities of the above equations and the spin indices have been neglected. Based on the infinite GMPS representation of  $\mathcal{A}$ , the Green's functions (or any multi-time impurity correlations) can be calculated in two steps: (1) Obtaining the transfer matrix by integrating each pair of Grassmann variables a and  $\bar{a}$  in one unit cell with the measure  $d\bar{a}dae^{-\bar{a}a}$  (which boils down to contracting the two physical indices of the two site tensors corresponding to a and  $\bar{a}$  [3], here we also note that this transfer matrix is completely different from the transfer matrix used when preparing an infinite MPS into the canonical form [11]), and then calculating the dominant left and right eigenstates of it, denoted as  $\langle v_l |$  and  $|v_r\rangle$  respectively, with dominant eigenvalue denoted as  $\lambda_{\max}$ ; (2) Identifying a finite window from the infinite GMPS representation of the ADT, and then evaluating the expectation value similar to the finite case, but using  $\langle v_l |$  and  $|v_r\rangle$  as left and right boundaries instead of trivial boundaries. These two steps are schematically shown in Fig. S2(a, b) respectively.

### S.III. INFINITE GMPS COMPRESSION

The multiplication of two MPSs with bond dimensions  $\chi_1$  and  $\chi_2$  will result in an MPS with bond dimension  $\chi_1\chi_2$ . In practice one sets a maximum bond dimension  $\chi$  and compress the resulting MPS into bond dimension  $\chi$  to maintain the computational cost [12]. The compression can be done exactly (in principle) and efficiently if the MPS has an exact canonical form, which is

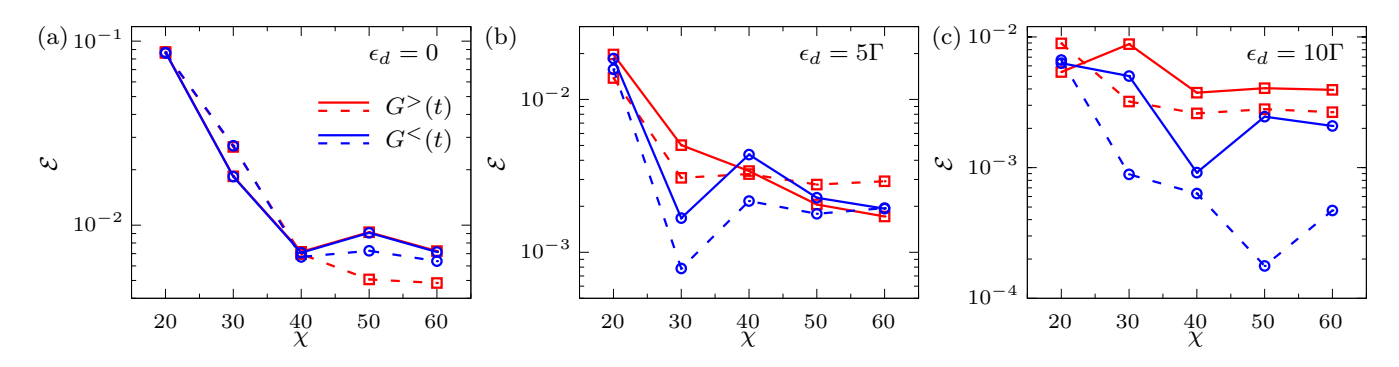


FIG. S3. Average error between the iGTEMPO results and ED results for (a)  $\epsilon_d/\Gamma=0$ , (b)  $\epsilon_d/\Gamma=5$  and (c)  $\epsilon_d/\Gamma=10$ . The red solid and dashed lines represent the iGTEMPO results for the equilibrium greater Green's functions calculated using SVD compression and IDMRG compression respectively. The blue solid and dashed lines represent the iGTEMPO results for the equilibrium lesser Green's functions calculated using SVD compression and IDMRG compression respectively. We have used  $\Gamma \delta t=0.005$  and  $\beta=40$  in all these simulations.

the case for both the open boundary MPS and the infinite boundary MPS. When performing compression of an infinite GMPS, the GMPS can be treated as a standard infinite MPS [3]. There already exists a number of algorithms to compress an infinite MPS, the representative ones include the deterministic SVD compression by performing a full left-to-right and then right-to-left sweep [11], and the iterative ones such as using the infinite density matrix renormalization group (IDMRG) algorithm [13], or the variational uniform MPS (VUMPS) algorithm [14], with one-to-one correspondence to their open boundary MPS counterparts. In this work, we have considered two approaches, the SVD compression and the IDMRG compression. The advantage of the first approach is that it is deterministic and in principle leads to the optimal canonical form. However, in the TTI-IF algorithm as described in Sec. S.I, one needs to multiply two same infinite GMPS with bond dimension  $\chi$ , as a result the resulting infinite GMPS has a bond dimension  $\chi^2$ , and the cost of the SVD compression will scale as  $O(\chi^6)$  as similar to the finite case [4] (but without the prefactor N for the total evolution time). Moreover, one needs to perform the inversion of the singular matrix (See Ref. [11] for details), which is numerical unstable if the conditional number of the singular matrix is too large (which is often the case, unfortunately). In comparison, the IDMRG algorithm is iterative (which means that one may be trapped in non-optimal infinite GMPS approximations), while its computational cost for our problem only scales as  $O(\chi^4)$  (in the iterative compression scheme, the multiplication of the infinite GMPSs are only computed on the fly to reduce the memory usage and the computational cost). In this work we use the single-site IDMRG algorithm following the implementation in the package MPSKit.jl [15]. When using the single-site IDMRG algorithm for our  $\mathbb{Z}_2$  symmetric MPS, the virtual space will be fixed from the beginning. Since we only have two symmetry sectors 0 and 1, we initialize each symmetry sector with size  $\chi/2$  and find that this is a good choice in practice. We typically use 10000 to 30000 IDMRG sweeps in the numerical simulations of the main text, since IDMRG essentially uses the power method to find the fixed point of the environment which generally converges quite slowly. We observe that the IDMRG compression is almost never trapped in very bad solutions as long as the bond dimension is large enough. In the future, one may use the more recent VUMPS algorithm for infinite GMPS compression, which may achieve faster convergences.

In Fig. S3 we show the convergence of the iGTEMPO calculations against the increase of the bond dimension, and compare the accuracy of the two approaches (SVD compression and IDMRG) used for infinite GMPS compression. We use the average error  $\mathcal{E}$ , defined as  $\mathcal{E}(\vec{x}, \vec{y}) = \sqrt{||\vec{x} - \vec{y}||^2/L}$  for two vectors  $\vec{x}$  and  $\vec{y}$  of length L, to quantify the derivation between the iGTEMPO results and the exact solutions calculated by exact diagonalization (ED). For SVD compression we have set the tolerance of the eigensolver (used to calculate the dominate eigenstates of the transfer matrix) to be  $10^{-14}$ , and for IDMRG we have used 20000 sweeps. We can see that in both approaches the average errors can be brought down to less than 1% with  $\chi=60$  for very different values of  $\epsilon_d$ , and the IDMRG results for  $\epsilon_d/\Gamma=0$ , 10 are slightly more accurate.

<sup>[1]</sup> J. Thoenniss, M. Sonner, A. Lerose, and D. A. Abanin, Phys. Rev. B 107, L201115 (2023).

<sup>[2]</sup> M. T. Fishman and S. R. White, Phys. Rev. B 92, 075132 (2015).

<sup>[3]</sup> R. Chen, X. Xu, and C. Guo, Phys. Rev. B 109, 045140 (2024).

<sup>[4]</sup> C. Guo and R. Chen, arXiv:2402.14350 (2024).

<sup>[5]</sup> S. L. Marple Jr, Digital spectral analysis (Courier Dover Publications, 2019).

<sup>[6]</sup> M. P. Zaletel, R. S. K. Mong, C. Karrasch, J. E. Moore, and F. Pollmann, Phys. Rev. B 91, 165112 (2015).

<sup>[7]</sup> A. Croy and U. Saalmann, Phys. Rev. B 80, 073102 (2009).

<sup>[8]</sup> X. Zheng, J. Jin, S. Welack, M. Luo, and Y. Yan, J. Chem. Phys. 130, 164708 (2009).

- [9] J. Hu, R.-X. Xu, and Y. Yan, J. Chem. Phys. 133, 101106 (2010).
- [10] I. Vilkoviskiy and D. A. Abanin, arXiv:2307.15592 (2023).
- [11] R. Orús and G. Vidal, Phys. Rev. B 78, 155117 (2008).
- [12] U. Schollwöck, Ann. Phys. **326**, 96 (2011).
- [13] I. P. McCulloch, arXiv:0804.2509 (2008).
- [14] V. Zauner-Stauber, L. Vanderstraeten, M. T. Fishman, F. Verstraete, and J. Haegeman, Phys. Rev. B 97, 045145 (2018).
- [15] https://github.com/maartenvd/MPSKit.jl.